Research Article

Journal of PeptideScience

Received: 1 October 2010 Revised: 1 November 2010 Accepted: 7 November 2010 Published online in Wiley Online Library: 20 December 2010

(wileyonlinelibrary.com) DOI 10.1002/psc.1339

Impact on the replacement of Phe by Trp in a short fragment of Aβ amyloid peptide on the formation of fibrils‡

Nitin Chaudhary and Ramakrishnan Nagaraj*

$A\beta_{16-22}$ (Ac-KLVFFAE-NH_2) is one of the shortest amyloid fibril-forming sequences identified in β-amyloid peptide. At neutral pH, the peptide forms fibrils in the concentration range of 0.2–2.0 mM after ≥10 days of incubation. Structures of the fibrils proposed based on solid-state NMR and MD simulations studies suggest antiparallel arrangement of β-strands and aromatic interactions between the Phe residues. In an effort to examine the role of aromatic interactions between two Phe residues in $A\beta_{16-22}$, we have studied the self-assembly of $A\beta_{16-22}$ (AβFF) and two of its variants, Ac-KLVFWAE-NH_2 (AβFW) and Ac-KLVWFAE-NH_2 (AβWF). The peptides were dissolved in methanol (MeOH) at a concentration of 1 mM and in water (AβFW and AβWF, 1 mM; AβFF, 330 μM). Peptide solutions (100 μM) were prepared in 50 mM sodium phosphate buffer at pH 7 by diluting from MeOH and water stock solutions. AβFW forms amyloid-like fibrils immediately from MeOH, as indicated by atomic force microscopy. Dilution of AβFW into phosphate buffer from stock solution prepared in MeOH results in fibrils, but with different morphology and dimensions. The secondary structure potentiated by MeOH seems to be important for the self-assembly of AβFW, as fibrils are not formed from water where the peptide is unordered. On the other hand, AβFF and AβWF do not form amyloid fibrils rapidly from any of the solvents used for dissolution. However, drying of AβWF from MeOH on mica surface gives rod-like and fibrous structures. Our study indicates that positioning of the aromatic residues F and W has an important role to play in promoting self-assembly of the $A\beta_{16-22}$ peptides. Copyright © 2010 European Peptide Society and John Wiley & Sons, Ltd.

Keywords: amyloid-forming peptide; aromatic interactions; peptide structure; peptide self-assembly

Introduction

Presence of extracellular amyloid plaques has long been associated with neuropathology of Alzheimer's disease. Amyloid plaques are formed by Aβ, which are 40–42 residue peptides produced by endoproteolytic cleavage of amyloid precursor protein (APP), a ubiquitously expressed type I membrane integral glycoprotein. In non-amyloidogenic pathway, APP is cleaved by α-secretase between Lys16 and Leu17 of Aβ peptide, thereby destroying the amyloidogenic sequence [1]. In the amyloidogenic pathway, β-secretase cleaves at *N*-terminus of the first residue of Aβ. Subsequent γ-secretase activity results in Aβ peptides with 39–43 amino acids, where Aβ40 and Aβ42 are the predominant alloforms [1,2].

Short peptide sequences from amyloidogenic proteins have been shown to form amyloid fibrils in isolation, making them good models for understanding the self-assembly of amyloidogenic proteins [3–12]. Short sequences that form amyloid fibrils *in vitro* under appropriate conditions have also been identified from Aβ [3,4,13,14]. $A\beta_{16-22}$ is among the shortest sequences from Aβ that form amyloid fibrils in aqueous solutions at neutral pH [4]. Solid-state NMR and MD simulations (MDS) studies have suggested in-register, antiparallel arrangement of β-strands in $A\beta_{16-22}$ fibrils [4,15]. Antiparallel, in-register β-sheet configuration has also been established in solution by isotope-edited IR spectroscopy [16]. Computer simulation studies suggest that monomeric $A\beta_{16-22}$ adopts predominantly random-coil conformation but self-assembles to form oligomers having antiparallel β-strands [17,18]. $A\beta_{16-22}$ forms amyloid fibrils around neutral pH, but self-assembles into helical ribbons and nanotubes under acidic conditions [19–21].

Frequent occurrence of aromatic residues in several unrelated amyloidogenic peptides suggests an important role of aromatic interactions in amyloid formation [4,6,7,22,23]. It is presumed that aromatic residues play an important role in self-assembly and affect the kinetics and stability of amyloid fibrils through stacking interactions [24–28]. The designed aromatic dipeptides have been shown to form a variety of nanostructures through π-stacking [29,30]. Studies with $A\beta_{16-22}$ and its analogs point to the importance of aromatic interactions in their self-assembly [27,28]. We have previously studied the self-assembly of two amyloidogenic peptides, $tau_{306-311}$ and β_2m_{59-71} in organic solvents and found that the self-assembled structures were greatly influenced by these solvents [31,32]. In fact, highly ordered non-fibrillar nanostructures could be obtained from the aromatic rich peptide, β_2m_{59-71} [32]. In order to examine if there is a positional preference for the occurrence of aromatic residues in the formation of fibrils or other self-assembled structures, we examined the

* *Correspondence to: Ramakrishnan Nagaraj, Centre for Cellular and Molecular Biology, Council of Scientific and Industrial Research, Uppal Road, Hyderabad 500 007, India. E-mail: nraj@ccmb.res.in*

Centre for Cellular and Molecular Biology, Council of Scientific and Industrial Research, Uppal Road, Hyderabad 500 007, India

‡ *Special issue devoted to the E-MRS Symposium C "Peptide-based materials: from nanostructures to applications", 7–11 June 2010, Strasbourg, France.*

self-assembly of $A\beta_{16-22}$ sequence and two of its variants, Ac-KLVFWAE-NH_2 ($A\beta$FW) and Ac-KLVWFAE-NH_2 ($A\beta$WF) in methanol (MeOH) and aqueous solutions.

Materials and Methods

Materials

Fmoc amino acids were purchased from Advanced ChemTech (Louisville, KY, USA) and Novabiochem AG (Laufelfingen, Switzerland). Peptide synthesis resin, PAL resin (5-(4-aminomethyl-3,5-dimethoxyphenoxy)valeric acid resin), was purchased from Advanced ChemTech (Louisville, KY, USA). All other reagents were of highest grade available.

Peptide Synthesis

The peptides, $A\beta$FF (Ac-KLVFFAE-NH_2), $A\beta$FW, and $A\beta$WF were synthesized using standard Fmoc chemistry [33]. The synthesized peptides were cleaved from the resin and deprotected using a mixture containing 82.5% TFA, 5% phenol, 5% H_2O, and 2.5% ethanedithiol for 12–15 h at room temperature [34]. Peptides were precipitated in ice-cold diethyl ether and purified on Hewlett Packard 1100 series HPLC (Hewlett-Packard, Waldbronn, Germany) instrument on a reversed-phase C18 Bio-Rad column (Bio-Rad, Richmond, CA, USA) using a linear gradient of H_2O and acetonitrile (0–100% acetonitrile) containing 0.1% TFA. Purified peptides were characterized using MALDI–TOF MS on a Voyager DE STR mass spectrometer (PerSeptive Biosystems, Foster city, CA, USA). The m/z value observed for $A\beta$FF was 894.52 (calculated mass: 894.03 Da) while m/z of 933.47 was obtained for both $A\beta$FW and $A\beta$WF (calculated mass: 933.07 Da). After purification, the solvent (H_2O–acetonitrile mixture containing 0.1% TFA) was evaporated and the peptides were stored as dry solids.

Peptide Solutions

Peptide stock solutions were prepared in H_2O and MeOH. The concentration of all the three peptides was 1 mM in MeOH. In H_2O, 1 mM stock solutions were prepared for $A\beta$FW and $A\beta$WF. Due to low solubility in H_2O, the concentration of the stock solution for $A\beta$FF was 330 μM. Solutions at 100 μM concentration were prepared in 50 mM phosphate buffer at pH 7.0 from H_2O and MeOH stock solutions. Concentrations of the peptides were estimated using a molar absorption coefficient of 286 M^{-1} cm^{-1} at 254 nm for $A\beta$FF, and 5690 M^{-1} cm^{-1} at $\lambda = 280$ nm for $A\beta$FW and $A\beta$WF.

Atomic Force Microscopy

Atomic force microscopy (AFM) imaging was carried out for freshly prepared peptide stock solutions in H_2O, MeOH, and for 100 μM peptide samples in 50 mM phosphate buffer at pH 7.0. For AFM, the peptides were deposited on freshly peeled mica surfaces. For peptide samples deposited from phosphate buffer, the mica pieces were washed gently with 40 μl deionized water after 10 min of peptide deposition and excess solution was removed through the edge of mica using tissue paper. The peptide samples deposited from MeOH were not washed. All the samples were air-dried before imaging. The images were acquired using tapping mode AFM (Multimode, Digital Instruments, Santa Barbara, CA, USA). A silicon nitride probe was oscillated at 275–310 kHz and images were collected at an optimized scan rate. Analysis was done using Nanoscope (R) III 5.30 r1 software (Digital Instruments, Santa Barbara, CA, USA). All the images are second-order flattened and presented in the height mode.

Dynamic Light Scattering

Dynamic light scattering (DLS) studies were carried out at 25 °C using Photocor Complex – DLS instrument (Photocor Instruments, College Park, MD, USA). A laser of wavelength 632.8 nm was used for collecting the data. Peptide stock solutions (1 mM for $A\beta$FW and $A\beta$WF, 1 mM for $A\beta$FF in MeOH and 330 μM in H_2O) and 100 μM peptide solutions in MeOH and in 50 mM phosphate buffer at pH 7.0 were examined immediately after sample preparation and after 5 days of incubation at room temperature. Autocorrelation functions (120) were measured 30 s apart for each sample. The data were processed using DynaLS software (V. 2.8.3) (Photocor Instruments, College Park, MD, USA) after discarding the rare outliers from the data which were ten or less. Data were recorded for MeOH and buffer blanks as controls. The scattering intensity for control solvents was very low and no decay in autocorrelation functions was observed.

Thioflavin T Fluorescence Spectroscopy

Thioflavin T (ThT) fluorescence spectra were recorded on Fluorolog-3 Model FL3-22 spectrofluorometer (Horiba Jobin Yvon, Park Avenue Edison, NJ, USA). Peptide samples (100 μM) prepared in 50 mM phosphate buffer at pH 7.0, were incubated at room temperature for 6 days. ThT fluorescence spectra of 6 days old samples were recorded in 10 μM ThT solution in 50 mM phosphate buffer at pH 7.0. Briefly, the peptide samples were diluted to 50 μM in 20 μM ThT solution prepared in 50 mM phosphate buffer at pH 7.0 such that the final ThT concentration is 10 μM. The excitation wavelength was set at 450 nm, slit width at 2 nm, and emission slit width at 5 nm.

CD Spectroscopy

Far-UV CD spectra of the peptides were recorded in H_2O, MeOH, and 50 mM phosphate buffer at pH 7.0 on Jasco J-815 spectropolarimeter (Jasco, Tokyo, Japan). Spectra were recorded for freshly dissolved 100 μM peptides in H_2O, MeOH, and in 50 mM phosphate buffer at pH 7.0 into which peptides were diluted from the stock solutions in H_2O and MeOH. The samples were kept at room temperature and after 5 days of incubation, CD spectra were recorded again. In H_2O and phosphate buffer, spectra were recorded from 250 to 190 nm. In MeOH, spectra could not be recorded at wavelengths below 195 nm because of the high absorbance at lower wavelengths. All the spectra were recorded in 0.1 cm path length cell using a step size of 0.2 nm, band width of 1 nm, and scan rate of 100 nm min^{-1}. The spectra were recorded by averaging ten scans and corrected by subtracting the solvent/buffer spectra. Mean residue ellipticity (MRE) was calculated using the formula: $[\theta]_{MRE} = (M_r \times \theta_{mdeg})/(100 \times l \times c)$, where M_r is mean residue weight, θ_{mdeg} is ellipticity in millidegrees, l is path length in decimeter, and c is the peptide concentration in mg ml^{-1}.

Fourier Transform IR Spectroscopy

Fourier transform IR (FTIR) spectra were recorded on a Bruker Alpha-E spectrometer (Bruker, Ettlingen, Germany) with Eco-attenuated total reflection (ATR) single reflection ATR sampling

Journal of PeptideScience

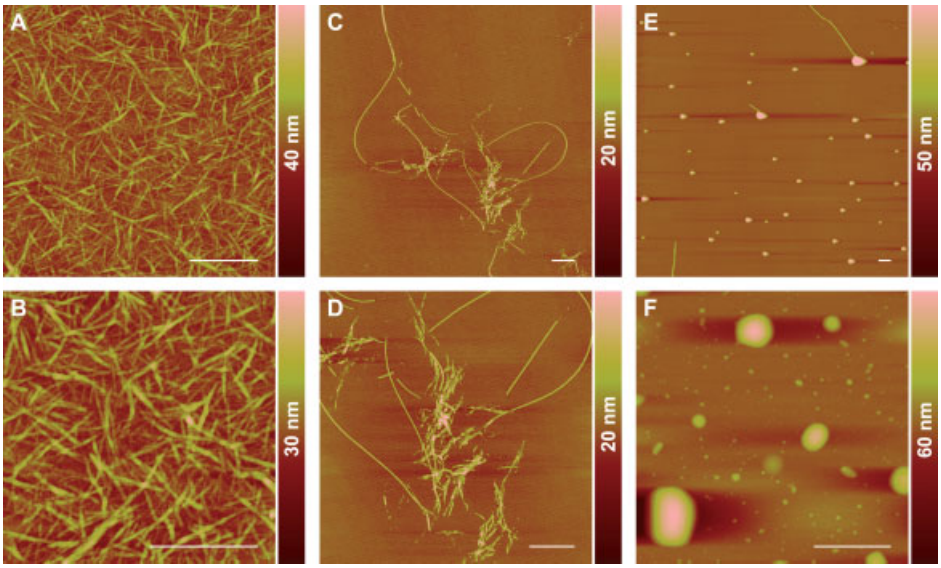

Figure 1. Self-assembled structures of AβFW after drying on mica. AFM images of AβFW (A, B), after drying on mica from MeOH; (C, D), from phosphate buffer into which peptide was diluted from MeOH; and (E, F), from phosphate buffer into which peptide was diluted from H_2O. Scale bars represent 1 μm.

module equipped with ZnSe ATR crystal. Peptide solutions (1 mM) were prepared in MeOH without exchanging TFA counterions. Peptides were spread out and dried as films on ZnSe crystal and ATR–FTIR spectra were recorded. Each spectrum is the average of 24 FTIR spectra at a resolution of 4 cm^{-1}.

Trp Fluorescence Spectroscopy

Steady-state Trp fluorescence spectra were recorded for AβFW and AβWF on Fluorolog-3 Model FL3-22 spectrofluorometer (Horiba Jobin Yvon). Spectra were recorded for 100 μM peptide solutions prepared in MeOH and in 50 mM phosphate buffer at pH 7.0. The peptides in phosphate buffer were diluted from 1 mM stock solutions prepared in MeOH. Spectra were recorded immediately after preparing the peptide solutions and after 6 days of incubation at room temperature. The excitation wavelength was set at 294 nm, slit width at 2 nm, and emission slit width at 5 nm.

Results

Atomic Force Microscopy

AFM imaging was carried out for freshly prepared peptide samples. Images were recorded for peptide stock solutions prepared in H_2O, MeOH, and 100 μM solutions prepared in 50 mM phosphate buffer at pH 7.0 from MeOH and H_2O solutions. Figure 1 shows images for AβFW when dried from MeOH (Panels A and B), from phosphate buffer into which peptide was diluted from MeOH (Panels C and D) and from phosphate buffer into which peptide was diluted from H_2O stock (Panels E and F). When dried from MeOH, AβFW forms fibrillar aggregates that range from 100 to 500 nm in length and 4–15 nm in diameter (Panels A and B). Fibrils were also observed from freshly dissolved AβFW in MeOH at much lower concentration of 150 μM (data not shown). When diluted into phosphate buffer at pH 7.0 from MeOH stock solution, long (up to 10 μm) fibrils are formed. Shorter fibrils (<0.5 μm) are also present (Panels C and D). Most fibrils are 4–10 nm in diameter. Imaging with AβFW that was diluted into phosphate buffer from H_2O shows spherical aggregates ranging from 2 to 50 nm in diameter (Panels E and F). Very few fibrillar structures, 8–10 nm thick, were also observed associated with the spherical aggregates (Panel E). AFM imaging of AβFF dried on mica from MeOH and 50 mM phosphate buffer at pH 7.0 did not show aggregates (data not shown). The self-assembly of $Aβ_{16-22}$ into amyloid fibrils requires several days [4]. The data shows rapid fibrillation of the peptide if FF in $Aβ_{16-22}$ is replaced with FW.

Imaging of AβWF is shown in Figure 2. The peptide shows large clumps when dried on mica from MeOH (Panels A and B). These clumps appear to be composed of short rod-like structures. Apart from the large clumps and short rods, thin fibrous structures ~3–7 nm in diameter were also present in the same sample but in different regions of the mica surface (Panels C and D). When imaging was performed with AβWF which was diluted into phosphate buffer from MeOH, no ordered aggregates were found. Very few amorphous-looking aggregates were present (Panels E and F). AβWF diluted from water stock into buffer shows spherical particles up to 100 nm in diameter but no fibrillar structures were observed (Panels G and H).

When imaging was carried out after drying the peptides from stock solutions in water, no ordered aggregates were observed (data not shown). In order to examine whether the peptides exist as aggregates or tend to aggregate in MeOH, DLS studies were carried out.

Dynamic Light Scattering

DLS studies were carried out at 25 °C for the peptides in MeOH and in 50 mM phosphate buffer at pH 7.0 immediately after preparing the solutions and after 5 days of incubation at room temperature. Figure 3 shows the intensity *versus* hydrodynamic radius plots for AβFW in MeOH. Solid and dotted lines show hydrodynamic radii distribution obtained for 100 μM and 1 mM AβFW solutions, respectively, immediately after preparing the samples. The aggregates are <100 nm when DLS was performed at 100 μM concentration (solid line). At 1 mM concentration, the distribution maximum is not altered but a significant proportion of the aggregates lies within 100–200 nm (dotted line). No significant difference was observed in hydrodynamic radii distribution after

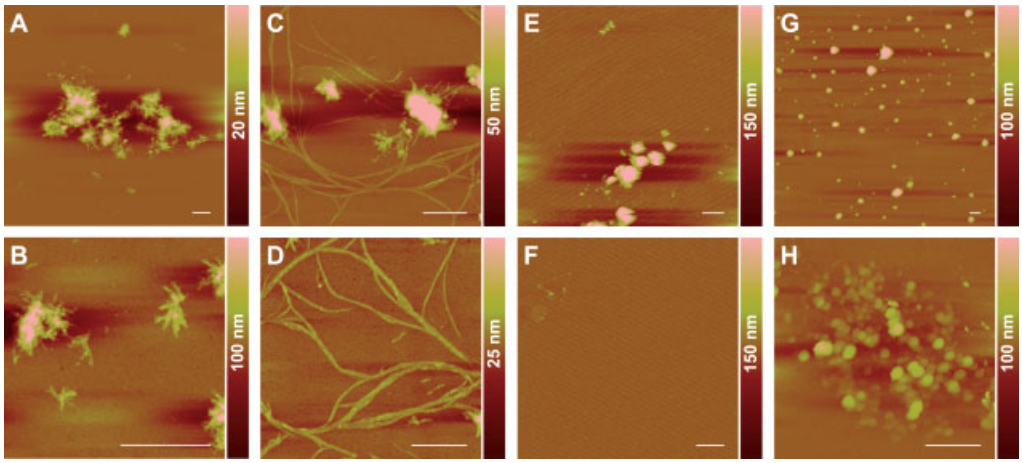

Figure 2. Self-assembled structures of AβWF after drying on mica. AFM images of AβWF (A–D), after drying on mica from MeOH; (E, F), from phosphate buffer into which peptide was diluted from MeOH; and (G, H), from phosphate buffer into which peptide was diluted from H_2O. Scale bars represent 1 μm.

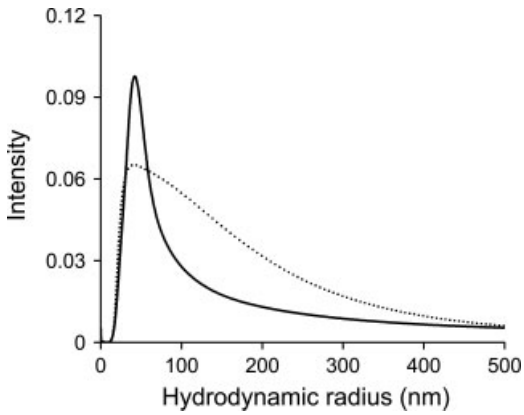

Figure 3. Hydrodynamic radii of AβFW aggregates in MeOH. Intensity against hydrodynamic radius plots, calculated using DLS data obtained for AβFW at different peptide concentrations immediately after dissolution in MeOH. (———), 100 μM and (· · · ·), 1 mM.

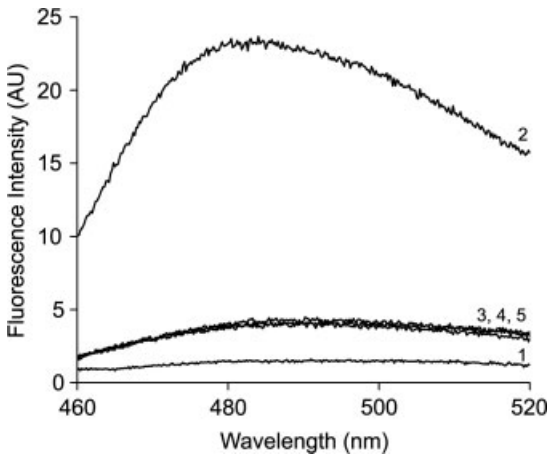

Figure 4. ThT fluorescence spectroscopy. Fluorescence of ThT (10 μM) in the presence of peptides that were incubated in 50 mM phosphate buffer at pH 7.0 at room temperature for 6 days. Spectrum 1, without peptide; spectrum 2, AβFW diluted from MeOH; spectrum 3, AβFW diluted from H_2O; spectrum 4, AβWF diluted from MeOH; and spectrum 5, AβWF diluted from H_2O.

5 days of incubation of 1 mM AβFW in MeOH (data not shown). Autocorrelation functions obtained for AβFF and AβWF in MeOH had significant contribution from the solvent autocorrelation function due to small scattering intensity caused by the peptides. Size determination from such autocorrelation functions is not reliable. At 100 μM concentration, the aqueous samples did not cause sufficient scattering required for size determination. These results suggest that AβFW forms aggregates in the MeOH and morphology of these aggregates is altered when diluted into the aqueous buffer.

As the peptides are analogs of the amyloid-forming peptide, $A\beta_{16-22}$, ThT fluorescence was used to examine if the aggregates formed by AβFW and AβWF are amyloid in nature.

ThT Fluorescence Spectroscopy

ThT fluorescence spectra were recorded for 100 μM peptide samples incubated in 50 mM phosphate buffer at pH 7.0 for 6 days. The spectra were recorded at 50 μM peptide concentration in 10 μM ThT solution prepared in 50 mM phosphate buffer at pH 7.0 (Figure 4). Spectrum 1 represents ThT fluorescence without peptide. Spectrum 2 shows ~15-fold enhancement in ThT fluorescence in the presence of AβFW which was diluted into buffer from MeOH. Traces 3, 4, and 5 represent spectra obtained in the presence of AβFW which was diluted into buffer from H_2O and AβWF samples diluted into buffer from MeOH and H_2O, respectively. No appreciable enhancement in ThT fluorescence was observed. The data show that AβFW forms amyloid fibrils in 50 mM phosphate buffer at pH 7.0 when diluted from MeOH, but no fibrils are formed when peptide is diluted into buffer from stock solution prepared in H_2O, even after 6 days of incubation. This indicates that the fibrils obtained from AβFW, when dried from MeOH, could arise due to ability of the peptide to aggregate in MeOH. The structure of the fibrils appears to be modulated when diluted into aqueous buffer (Figure 1(A)–(D)). AβWF does not cause enhancement in ThT fluorescence when diluted into phosphate buffer from either of the solvents. This suggests that the rods and fibers formed by AβWF, as observed by AFM imaging (Figure 2(A)–(D)), may not be classical amyloid fibrils.

AβFF does not cause any enhancement in ThT fluorescence after 6 days of incubation in 50 mM phosphate buffer at pH 7.0 (data not shown). This further shows that the F20 → W substitution renders

Journal of PeptideScience

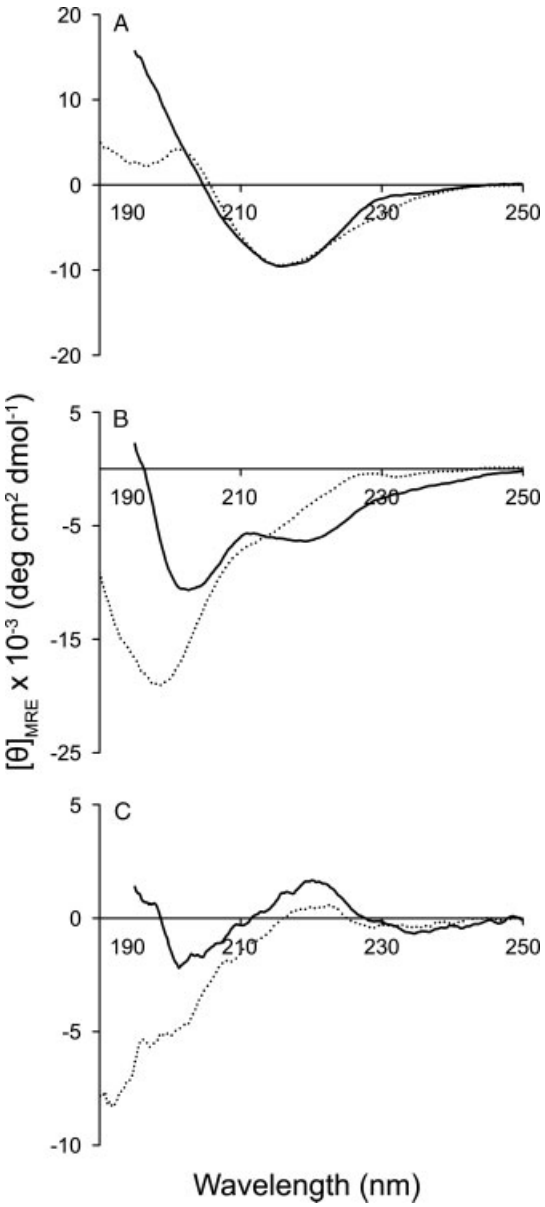

Figure 5. Conformations of freshly prepared peptide solutions. Far-UV CD spectra of 100 μM peptides immediately after dissolution in MeOH (———) and in 50 mM phosphate buffer at pH 7.0 when diluted from MeOH (· · · ·); (A), AβFW; (B), AβWF; and (C), AβFF.

the peptide AβFW highly amyloidogenic. The conformations of the peptides in solution and in the solid state were studied in order to examine the correlation among ThT fluorescence, the morphology of the self-assembled structures, and the conformations of the peptides.

CD Spectroscopy

For CD experiments, freshly prepared peptide stock solutions were diluted to 100 μM concentration in the same solvent and in 50 mM phosphate buffer at pH 7.0. Figure 5 shows the CD spectra recorded immediately after preparing the samples. In H_2O and in buffer into which peptides are diluted from H_2O, all the peptides adopt random conformation (data not shown). However, the peptides are structured in MeOH. Solid and dotted lines represent spectra recorded in MeOH and in phosphate buffer, respectively. AβFW adopts β-structure in MeOH and the structure is retained upon dilution into the buffer (Panel A). AβWF populates an ensemble of turn and β-conformations in MeOH, but becomes unstructured when diluted into phosphate buffer (Panel B). AβFF shows negative bands at ~235 and 202 nm and a positive band ~220 nm in MeOH (solid line, Panel C). Similar spectra have been suggested as β-turn-like arrangement [35]. When diluted into the phosphate buffer, the peptide largely adopts random-coil conformation (dotted line, Panel C). CD spectra were also recorded after 5 days incubation of the samples at room temperature (data not shown). The structural components of AβFW are not significantly altered even after 5 days of incubation in MeOH and H_2O. In phosphate buffer, there was an increase in the β-content for the peptide that was diluted into the buffer from H_2O. Conformations of AβFF and AβWF remain largely unchanged after 5 days of incubation.

CD spectroscopy shows that AβFW adopts largely β-structure in MeOH (solid line, Figure 5(A)) and forms fibrillar structures as observed by AFM after drying on mica (Figure 1(A) and (B)). When diluted into phosphate buffer from MeOH, the peptide adopts β-structure (dotted line, Figure 5(A)) and causes enhancement in ThT fluorescence (Figure 4), suggesting the presence of amyloid fibrils as observed using AFM (Figure 1(C) and (D)). AβWF, that populates an ensemble of turn and β-conformations in MeOH, showed ordered rod-like structures and few filaments when imaged with AFM (Figure 2(A)–(D)). ATR–FTIR spectra were recorded to ascertain the structures adopted by the peptides in dried films, when dried from MeOH.

FTIR Spectroscopy

Amide I region in FTIR spectra is sensitive to secondary structures of proteins and peptides, as it essentially arises from C═O stretching vibration with a small admixture of the NH bending [36]. The peptides were dried on ZnSe crystal from MeOH and ATR–FTIR spectra were recorded on dry peptide films to correlate the peptide secondary structures with self-assembled structures on mica (Figure 6). Amide I absorption bands centered at 1625, 1629, and 1626 cm^{-1} were observed for AβFW (Panel A), AβWF (Panel B), and AβFF (Panel C), respectively. These bands correspond to β-structure suggesting that the peptides are organized in β-structures in the rod-like, fibrillar, and other morphologies observed using AFM after drying the peptides from MeOH.

Trp Fluorescence Spectroscopy

Trp fluorescence is sensitive to its environment and could provide insights into the orientation of the aromatic residues in the self-assembled states of the AβFW and AβWF peptides. Steady-state Trp fluorescence spectra of AβFW and AβWF were recorded in MeOH and in 50 mM phosphate buffer at pH 7.0 into which the peptides were diluted from 1 mM stock solutions prepared in MeOH. The spectra shown in Figure 7 are those recorded immediately after preparing the samples. Solid and dotted lines represent spectra recorded in MeOH and in phosphate buffer, respectively. At identical concentrations, fluorescence intensity of AβFW is significantly less than that of AβWF in both MeOH and buffer. Further, fluorescence intensity of AβFW is lower in buffer as compared to that in MeOH (Panel A). In MeOH, fluorescence emission maximum for both the peptides is at ~341 nm (solid lines). The λ_{max} in phosphate buffer is at ~348 nm for both the peptides (dotted lines). Emission maximum at ~348 nm suggests

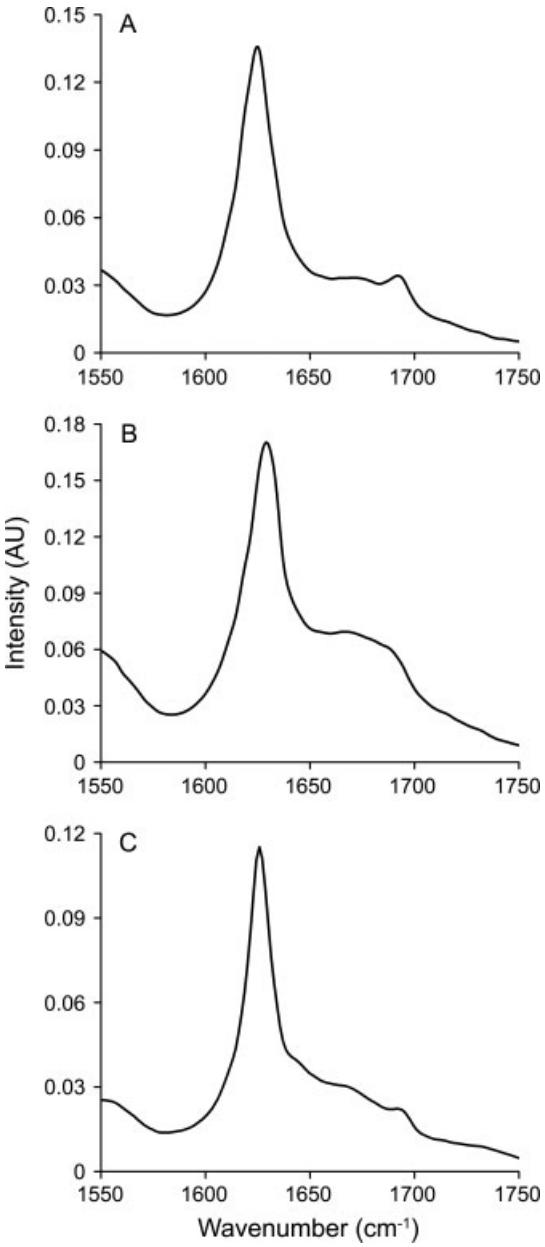

Figure 6. Conformations of the peptides in dried films. FTIR spectra of amide I region after drying the peptides from MeOH. (A), AβFW; (B), AβWF; and (C), AβFF. Peptide concentrations in MeOH were 1 mM.

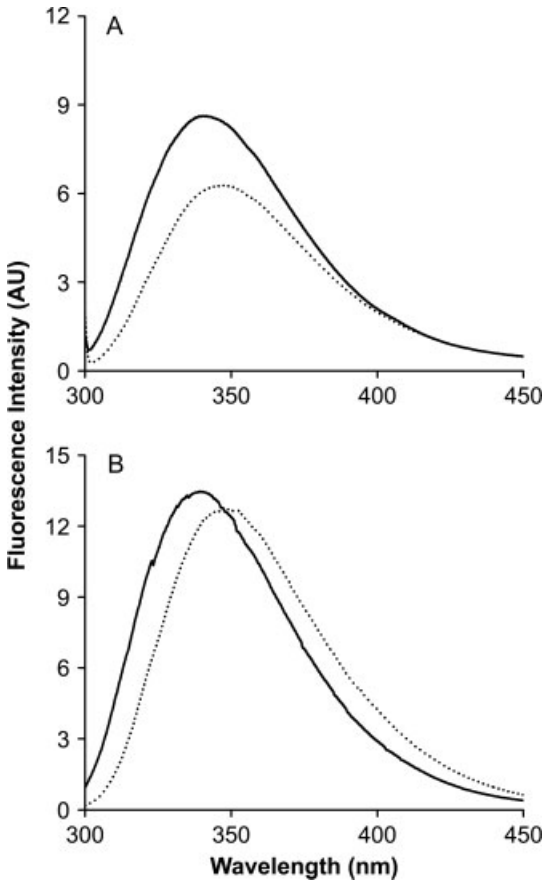

Figure 7. Trp fluorescence spectra of AβFW and AβWF. Trp fluorescence spectra of AβFW (Panel A) and AβWF (Panel B) in MeOH (———) and in 50 mM phosphate buffer at pH 7.0 into which the peptides were diluted from MeOH (· · · ·). The spectra were recorded immediately after preparing the samples. Peptide concentration was 100 µM.

that Trp residues of both AβFW and AβWF are exposed to the aqueous buffer. However, AβFW, that forms fibrillar aggregates has low fluorescence quantum yield as compared to that of AβWF. After 5 days of incubation at room temperature, no appreciable changes were observed in the fluorescence spectra (data not shown).

Discussion

Interactions between aromatic residues are observed in several areas of chemistry and biochemistry, especially in molecular recognition and self-assembly [29,30,35,37]. In proteins, aromatic–aromatic interactions are involved in stabilizing tertiary and quaternary structures [38–40]. Aromatic residues are also involved in CH$\cdots\pi$ interactions, and these interactions also contribute to the stability of protein structure [41]. Despite the low frequency of occurrence of aromatic residues in proteins, amyloidogenic stretches present in the proteins are frequently found to have aromatic residues [4,6,7,22,23]. β_2m$_{59-71}$, a highly aromatic rich peptide (6 of the 13 residues are aromatic), forms amyloid fibrils across a pH range of 1–7 suggesting that aromatic interactions might be involved in the self-assembly [7]. The peptide also forms a variety of non-amyloid structures [32]. Aβ_{16-22}, that constitutes the central core of Alzheimer's β-amyloid peptide, forms amyloid fibrils in isolation slowly. The peptide has an aromatic motif (KLV**FF**AE) and is among the shortest Aβ amyloidogenic sequences. The peptide has been shown to form amyloid fibrils after ten or more days of incubation when dissolved at 0.2–2.0 mM concentration in aqueous solutions or acetonitrile/H_2O mixture at neutral pH [4,20,42]. At acidic pH, the peptide forms highly ordered nanotubes in water and in acetonitrile/H_2O mixture [19,20,42]. At neutral pH, glutamate is negatively charged whereas lysine is positively charged, resulting in antiparallel fibril formation possibly to satisfy the charge complementarity [4]. At acidic pH, glutamate becomes uncharged, thereby giving amphiphilic character to the peptide. It has been argued that the amphiphilic character drives the peptide to self-assemble into nanotubes and aromatic interactions between Phe rings play an important role in Aβ_{16-22} self-assembly [19,42]. The antiparallel β-structure suggested for

Journal of PeptideScience

$A\beta_{16-22}$ fibrils by solid-state NMR hints at stacking interactions between F19 of adjacent strands of the same sheet [4,42]. F20 is unlikely to be involved in stacking interactions within the sheet. However, MDS studies suggest edge to face interaction between F19 and F20 that are present on different sheets [42]. Touchette *et al*. investigated $A\beta_{1-40}$ fibrils using $A\beta_{1-40}$ mutants where F4 and F19 were individually substituted with W [43]. It was shown that F19 → W mutation is easily tolerated and the peptide, $A\beta_{1-40}$ (F19W) forms fibrils very similar to those formed by $A\beta_{1-40}$ [43].

To understand the importance of aromatic interactions and positional preference of the aromatic residues in fibril formation, we studied the self-assembly of $A\beta_{16-22}$ and two analogs AβFW and AβWF in MeOH and in aqueous phosphate buffer at neutral pH. AβFW adopts β-structure in MeOH and amyloid-like fibrils were observed in AFM imaging after drying the peptide on mica. Dilution into phosphate buffer also shows amyloid fibrils. Although fibril formation in $A\beta_{16-22}$ takes several days, fibrils of AβFW were formed immediately after dissolution in MeOH at a concentration as low as 150 μM. AβFF and AβWF adopt an ensemble of β- and turn-structures in MeOH. AFM imaging of the dried AβWF shows short rod-like structures present in large clumps. Very few fibrous aggregates were also observed. ATR–FTIR spectra confirm that the peptides are in β-conformation in the dried films. This suggests that the fibrils obtained from AβFW on mica could be amyloid fibrils as they adopt β-structure and their morphology and thickness are characteristic of amyloid fibrils. Although AβFW adopts β-structure in MeOH, AβFF and AβWF adopt β-structure during drying process. Unlike AβFW, dilution of AβFF and AβWF into aqueous phosphate buffer from MeOH does not result in fibril formation as suggested by AFM imaging and ThT fluorescence assay. Although Phe19 → Trp substitution is easily tolerated in full length $A\beta_{1-40}$, amyloidogenicity is severely compromised in AβWF. This can be attributed to the orientation of the β-strands in the fibrils of the two peptides: $A\beta_{1-40}$ forms fibrils with parallel β-sheet arrangement while $A\beta_{16-22}$ fibrils have antiparallel orientation of the strands [4,44]. Further, a substitution is likely to be tolerated in a longer sequence as compared to the shorter one. F20 → W substitution, on the other hand, does not abrogate fibril formation by $A\beta_{16-22}$ as indicated by AβFW fibrillization. In fact, this substitution significantly enhances the amyloidogenicity of the peptide. These data suggest the importance of positional preference of F in the amyloid formation by $A\beta_{16-22}$. Apart from this, enhanced amyloidogenicity in AβFW (F20 → W substitution) might also be because of loss in amyloidogenicity control conferred by F20. Interestingly, as found by ThT fluorescence spectroscopy as well as by AFM imaging, AβFW does not form fibrils in phosphate buffer if diluted from stock solution prepared in H_2O, in which the peptide is largely unordered. The AβFW fibrils obtained after drying the peptide from MeOH were shorter (<1 μm long) than $A\beta_{16-22}$ fibrils reported in literature [4,20]. However, when diluted into phosphate buffer from MeOH and imaged by AFM, very long (up to tens of micrometers) fibrils were obtained. Self-assembly of AβFW is likely to be influenced by the low dielectric constant of MeOH which is known to influence the peptide structure [45,46]. Steady-state Trp fluorescence showed that AβFW and AβWF fluorescence emission maxima were identical, unlike $A\beta_{1-40}$ (F19W), which shows large blue shift in Trp fluorescence in the fibrillar form [43]. However, like $A\beta_{1-40}$ (F19W) fibrils, fluorescence quantum yield was significantly less for AβFW in MeOH as well as in phosphate buffer as compared to that for AβWF which can be attributed to excited-state quenching of Trp in AβFW fibrils. Brand and co-workers showed that a conserved Trp in several *Drosophila* homeodomains has unusually low fluorescence quantum yield [47,48]. The low quantum yield is attributed to the quenching due to excited-state NH$\cdots\pi$ bond involving Trp and an aromatic residue. In human interleukin-2, NH$\cdots\pi$ bond between W121 and F117 contributes to fluorescence quenching of the single Trp present in the protein [48]. Amyloid fibrils are highly ordered structures, and it is likely that W in AβFW fibrils is appropriately oriented for quenching by F. Quenching by amino group is more when it is protonated [49]. At neutral pH, *N*-terminus of the peptide as well as ε-NH_2 of Lys would be protonated. Presence of these quenchers in close proximity to W in AβFW fibrils would contribute to fluorescence quenching.

Importance of aromatic residues has been investigated in several amyloidogenic peptides. Ala-scanning study with amyloidogenic peptide, NFGAILSS from human amylin shows that Phe → Ala substitution abrogates fibril formation by the peptide [50]. Substitution of any other amino acid with Ala affects the kinetics of aggregation and morphology of the fibrils but does not abolish the ability to form amyloid fibrils [50]. However, Tracz *et al*. showed that the single Phe present in the amyloidogenic peptides from human amylin, $hIAPP_{10-19}$, $hIAPP_{21-29}$, and $hIAPP_{22-27}$ is not required for fibril formation [51]. Peptides in which Phe is substituted by Leu, form fibrils similar to the wild-type peptides. It has been argued that hydrophobicity and propensity to form β-structure is higher for F and L than those for A. Therefore, F → L substitution does not affect fibril formation, whereas F → A substitution completely abolishes it. Our data show that nearly identical peptides have drastically different amyloid propensities as also shown for amyloidogenic peptide from human amylin, NFGAILSS, and its variants where F is substituted with Y and W [52].

Our results indicate that the sequence in which F and W occur in the variants of $A\beta_{16-22}$ causes drastic change in the ability of the peptides to form amyloid fibrils. Eisenberg and coworkers [11] have obtained atomic resolution structures of unrelated short amyloid peptides and suggested steric zipper as the fundamental unit of these fibrils. These results suggest that apart from the aromatic interactions, interdigitation of the side chains between β-sheets is crucial for stable amyloid fold implying the importance of primary sequence. It is likely that the antiparallel arrangement of β-strands would allow proper orientation of aromatic residues to allow π-interactions and better stacking of the side chains in AβFW fibrils. This orientation of aromatic residues may not be favorable for AβWF in antiparallel orientation thereby reducing its amyloidogenicity. Another intriguing result is fibrillization of AβFW in aqueous phosphate buffer. The peptide causes enhancement in ThT fluorescence only when diluted from MeOH in which peptide adopts β-structure. When diluted from H_2O, no fibrillization was observed. Although there is only 5% MeOH present while performing ThT fluorescence assay, its effect on fibril formation cannot be ruled out. DLS studies indicate that AβFW aggregates in MeOH but no time-dependent increase in hydrodynamic radii was observed. DLS performed at higher peptide concentration (1 mM) shows size distribution shifted toward larger hydrodynamic radii as compared to 100 μM samples which may arise due to the presence of particles with larger size at higher peptide concentration. AβFF and AβWF in MeOH (1 mM), on the other hand, cause insignificant scattering of light as compared to the neat MeOH. However, drying the AβWF peptide on mica results in its aggregation. The differences in the structures observed for AβFF, AβFW, and AβWF by AFM could be related to their aggregation ability in MeOH. The observation of spherical aggregates by AFM in the case of AβFW and AβWF could arise due to the drying process, as DLS does

not indicate the presence of aggregates in aqueous solutions. Clearly, positioning of the aromatic residues has an important role to play in promoting self-assembly of the peptides. This study on Aβ_{16-22} and its analogs highlights the importance of aromatic stacking interactions and the solvent used for dissolution in the self-assembly of peptides to form fibrils.

Acknowledgements

We thank E. Bikshapathy for help in synthesis of the peptides. Funding from CSIR Network project NWP035 is gratefully acknowledged.

References

1 Hardy J. Amyloid, the presenilins and Alzheimer's disease. *Trends Neurosci.* 1997; **20**: 154–159.
2 Cappai R, White AR. Amyloid beta. *Int. J. Biochem. Cell Biol.* 1999; **31**: 885–889.
3 Tjernberg LO, Callaway DJ, Tjernberg A, Hahne S, Lilliehook C, Terenius L, Thyberg J, Nordstedt C. A molecular model of Alzheimer amyloid beta-peptide fibril formation. *J. Biol. Chem.* 1999; **274**: 12619–12625.
4 Balbach JJ, Ishii Y, Antzutkin ON, Leapman RD, Rizzo NW, Dyda F, Reed J, Tycko R. Amyloid fibril formation by A beta 16–22, a seven-residue fragment of the Alzheimer's beta-amyloid peptide, and structural characterization by solid state NMR. *Biochemistry* 2000; **39**: 13748–13759.
5 Balbirnie M, Grothe R, Eisenberg DS. An amyloid-forming peptide from the yeast prion Sup35 reveals a dehydrated beta-sheet structure for amyloid. *Proc. Natl. Acad. Sci. U.S.A.* 2001; **98**: 2375–2380.
6 Reches M, Porat Y, Gazit E. Amyloid fibril formation by pentapeptide and tetrapeptide fragments of human calcitonin. *J. Biol. Chem.* 2002; **277**: 35475–35480.
7 Jones S, Manning J, Kad NM, Radford SE. Amyloid-forming peptides from beta2-microglobulin-insights into the mechanism of fibril formation in vitro. *J. Mol. Biol.* 2003; **325**: 249–257.
8 Zanuy D, Ma B, Nussinov R. Short peptide amyloid organization: stabilities and conformations of the islet amyloid peptide NFGAIL. *Biophys. J.* 2003; **84**: 1884–1894.
9 Goux WJ, Kopplin L, Nguyen AD, Leak K, Rutkofsky M, Shanmuganandam VD, Sharma D, Inouye H, Kirschner DA. The formation of straight and twisted filaments from short tau peptides. *J. Biol. Chem.* 2004; **279**: 26868–26875.
10 Ivanova MI, Thompson MJ, Eisenberg D. A systematic screen of beta(2)-microglobulin and insulin for amyloid-like segments. *Proc. Natl. Acad. Sci. USA* 2006; **103**: 4079–4082.
11 Sawaya MR, Sambashivan S, Nelson R, Ivanova MI, Sievers SA, Apostol MI, Thompson MJ, Balbirnie M, Wiltzius JJ, McFarlane HT, Madsen AO, Riekel C, Eisenberg D. Atomic structures of amyloid cross-beta spines reveal varied steric zippers. *Nature* 2007; **447**: 453–457.
12 Hamley IW. Peptide fibrillization. *Angew. Chem. Int. Ed. Engl.* 2007; **46**: 8128–8147.
13 Halverson K, Fraser PE, Kirschner DA, Lansbury PT Jr. Molecular determinants of amyloid deposition in Alzheimer's disease: conformational studies of synthetic beta-protein fragments. *Biochemistry* 1990; **29**: 2639–2644.
14 Fraser PE, Nguyen JT, Surewicz WK, Kirschner DA. pH-dependent structural transitions of Alzheimer amyloid peptides. *Biophys. J.* 1991; **60**: 1190–1201.
15 Ma B, Nussinov R. Stabilities and conformations of Alzheimer's beta-amyloid peptide oligomers (Abeta 16–22, Abeta 16–35, and Abeta 10–35): Sequence effects. *Proc. Natl. Acad. Sci. U.S.A.* 2002; **99**: 14126–14131.
16 Petty SA, Decatur SM. Experimental evidence for the reorganization of beta-strands within aggregates of the Abeta(16–22) peptide. *J. Am. Chem. Soc.* 2005; **127**: 13488–13489.
17 Klimov DK, Thirumalai D. Dissecting the assembly of Abeta16-22 amyloid peptides into antiparallel beta sheets. *Structure* 2003; **11**: 295–307.
18 Favrin G, Irback A, Mohanty S. Oligomerization of amyloid Abeta16-22 peptides using hydrogen bonds and hydrophobicity forces. *Biophys. J.* 2004; **87**: 3657–3664.
19 Lu K, Jacob J, Thiyagarajan P, Conticello VP, Lynn DG. Exploiting amyloid fibril lamination for nanotube self-assembly. *J. Am. Chem. Soc.* 2003; **125**: 6391–6393.
20 Liang Y, Pingali SV, Jogalekar AS, Snyder JP, Thiyagarajan P, Lynn DG. Cross-strand pairing and amyloid assembly. *Biochemistry* 2008; **47**: 10018–10026.
21 Elgersma RC, Rijkers DT, Liskamp RM. pH controlled aggregation morphology of Abeta(16–22): formation of peptide nanotubes, helical tapes and amyloid fibrils. *Adv. Exp. Med. Biol.* 2009; **611**: 239–240.
22 Westermark GT, Engstrom U, Westermark P. The N-terminal segment of protein AA determines its fibrillogenic property. *Biochem. Biophys. Res. Commun.* 1992; **182**: 27–33.
23 Haggqvist B, Naslund J, Sletten K, Westermark GT, Mucchiano G, Tjernberg LO, Nordstedt C, Engstrom U, Westermark P. Medin: an integral fragment of aortic smooth muscle cell-produced lactadherin forms the most common human amyloid. *Proc. Natl. Acad. Sci. U.S.A.* 1999; **96**: 8669–8674.
24 Gazit E. A possible role for pi-stacking in the self-assembly of amyloid fibrils. *FASEB J.* 2002; **16**: 77–83.
25 Gazit E. Mechanisms of amyloid fibril self-assembly and inhibition. Model short peptides as a key research tool. *FEBS J.* 2005; **272**: 5971–5978.
26 Marek P, Abedini A, Song B, Kanungo M, Johnson ME, Gupta R, Zaman W, Wong SS, Raleigh DP. Aromatic interactions are not required for amyloid fibril formation by islet amyloid polypeptide but do influence the rate of fibril formation and fibril morphology. *Biochemistry* 2007; **46**: 3255–3261.
27 Krysmann MJ, Castelletto V, Hamley IW. Fibrillisation of hydrophobically modified amyloid peptide fragments in an organic solvent. *Soft Matter* 2007; **3**: 1401–1406.
28 Krysmann MJ, Castelletto V, Kelarakis A, Hamley IW, Hule RA, Pochan DJ. Self-assembly and hydrogelation of an amyloid peptide fragment. *Biochemistry* 2008; **47**: 4597–4605.
29 Reches M, Gazit E. Casting metal nanowires within discrete self-assembled peptide nanotubes. *Science* 2003; **300**: 625–627.
30 Reches M, Gazit E. Designed aromatic homo-dipeptides: formation of ordered nanostructures and potential nanotechnological applications. *Phys. Biol.* 2006; **3**: S10–S19.
31 Chaudhary N, Singh S, Nagaraj R. Morphology of self-assembled structures formed by short peptides from the amyloidogenic protein tau depends on the solvent in which the peptides are dissolved. *J. Pept. Sci.* 2009; **15**: 675–684.
32 Chaudhary N, Singh S, Nagaraj R. Organic solvent mediated self-association of an amyloid forming peptide from beta2-microglobulin: an atomic force microscopy study. *Biopolymers* 2008; **90**: 783–791.
33 Atherton E. *Solid Phase Synthesis: A Practical Approach*. IRL Press: Oxford, 1989.
34 King DS, Fields CG, Fields GB. A cleavage method which minimizes side reactions following Fmoc solid phase peptide synthesis. *Int. J. Pept. Protein Res.* 1990; **36**: 255–266.
35 Ma M, Kuang Y, Gao Y, Zhang Y, Gao P, Xu B. Aromatic–aromatic interactions induce the self-assembly of pentapeptidic derivatives in water to form nanofibers and supramolecular hydrogels. *J. Am. Chem. Soc.* 2010; **132**: 2719–2728.
36 Surewicz WK, Mantsch HH, Chapman D. Determination of protein secondary structure by Fourier transform infrared spectroscopy: a critical assessment. *Biochemistry* 1993; **32**: 389–394.
37 Claessens CG, Stoddart JF. pi–pi interactions in self-assembly. *J. Phys. Org. Chem.* 1997; **10**: 254–272.
38 Burley SK, Petsko GA. Aromatic–aromatic interaction: a mechanism of protein structure stabilization. *Science* 1985; **229**: 23–28.
39 Burley SK, Petsko GA. Amino–aromatic interactions in proteins. *FEBS Lett.* 1986; **203**: 139–143.
40 McGaughey GB, Gagne M, Rappe AK. pi–Stacking interactions. Alive and well in proteins. *J. Biol. Chem.* 1998; **273**: 15458–15463.
41 Brandl M, Weiss MS, Jabs A, Suhnel J, Hilgenfeld R. C-H. . .pi-interactions in proteins. *J. Mol. Biol.* 2001; **307**: 357–377.
42 Mehta AK, Lu K, Childers WS, Liang Y, Dublin SN, Dong J, Snyder JP, Pingali SV, Thiyagarajan P, Lynn DG. Facial symmetry in protein self-assembly. *J. Am. Chem. Soc.* 2008; **130**: 9829–9835.

43 Touchette JC, Williams LL, Ajit D, Gallazzi F, Nichols MR. Probing the amyloid-beta(1–40) fibril environment with substituted tryptophan residues. *Arch. Biochem. Biophys.* 2010; **494**: 192–197.
44 Balbach JJ, Petkova AT, Oyler NA, Antzutkin ON, Gordon DJ, Meredith SC, Tycko R. Supramolecular structure in full-length Alzheimer's beta-amyloid fibrils: evidence for a parallel beta-sheet organization from solid-state nuclear magnetic resonance. *Biophys. J.* 2002; **83**: 1205–1216.
45 Dwyer DS. Molecular simulation of the effects of alcohols on peptide structure. *Biopolymers* 1999; **49**: 635–645.
46 Kinoshita M, Okamoto Y, Hirata F. Peptide conformations in alcohol and water: analyses by the reference interaction site model theory. *J. Am. Chem. Soc.* 2000; **122**: 2773–2779.
47 Nanda V, Brand L. Aromatic interactions in homeodomains contribute to the low quantum yield of a conserved, buried tryptophan. *Proteins* 2000; **40**: 112–125.
48 Nanda V, Liang SM, Brand L. Hydrophobic clustering in acid-denatured IL-2 and fluorescence of a Trp NH-pi H-bond. *Biochem. Biophys. Res. Commun.* 2000; **279**: 770–778.
49 Beechem JM, Brand L. Time-resolved fluorescence of proteins. *Annu. Rev. Biochem.* 1985; **54**: 43–71.
50 Azriel R, Gazit E. Analysis of the minimal amyloid-forming fragment of the islet amyloid polypeptide. An experimental support for the key role of the phenylalanine residue in amyloid formation. *J. Biol. Chem.* 2001; **276**: 34156–34161.
51 Tracz SM, Abedini A, Driscoll M, Raleigh DP. Role of aromatic interactions in amyloid formation by peptides derived from human Amylin. *Biochemistry* 2004; **43**: 15901–15908.
52 Porat Y, Stepensky A, Ding FX, Naider F, Gazit E. Completely different amyloidogenic potential of nearly identical peptide fragments. *Biopolymers* 2003; **69**: 161–164.

